

PAPER

# Non-chemical fluorination of hexagonal boron nitride by high-energy ion irradiation

To cite this article: Shiro Entani *et al* 2020 *Nanotechnology* **31** 125705

View the [article online](#) for updates and enhancements.






**IOP | ebooks™**

Bringing together innovative digital publishing with leading authors from the global scientific community.

Start exploring the collection—download the first chapter of every title for free.

# Non-chemical fluorination of hexagonal boron nitride by high-energy ion irradiation

Shiro Entani<sup>1,9</sup> , Konstantin V Larionov<sup>2,3,8</sup>, Zakhar I Popov<sup>2,4</sup>, Masaru Takizawa<sup>5</sup>, Masaki Mizuguchi<sup>6</sup> , Hideo Watanabe<sup>7</sup>, Songtian Li<sup>1</sup>, Hiroshi Naramoto<sup>1</sup>, Pavel B Sorokin<sup>1,2,3,9</sup>  and Seiji Sakai<sup>1</sup>

<sup>1</sup>Quantum Beam Science Research Directorate, National Institutes for Quantum and Radiological Science and Technology, Takasaki, Gunma 370-1292, Japan

<sup>2</sup>National University of Science and Technology MISiS, Moscow 119049, Russia

<sup>3</sup>Moscow Institute of Physics and Technology, 9 Institutskii per, Dolgoprudny, Moscow Region, 141700, Russia

<sup>4</sup>Emanuel Institute of Biochemical Physics RAS, 4 Kosygina st, Moscow 199339, Russia

<sup>5</sup>Department of Physical Sciences, Faculty of Science and Engineering, Ritsumeikan University, Kusatsu, Shiga 525-8577, Japan

<sup>6</sup>Institute for Materials Research, Tohoku University, Aoba-ku, Sendai 980-8570, Japan

<sup>7</sup>Research Institute for Applied Mechanics, Kyushu University, Kasuga, Fukuoka 816-8580, Japan

<sup>8</sup>Technological Institute for Superhard and Novel Carbon Materials, Troitsk, Moscow 108840, Russia

E-mail: [entani.shiro@qst.go.jp](mailto:entani.shiro@qst.go.jp) and [PBSorokin@misis.ru](mailto:PBSorokin@misis.ru)

Received 18 September 2019, revised 31 October 2019

Accepted for publication 26 November 2019

Published 8 January 2020



CrossMark

## Abstract

Two-dimensional materials such as hexagonal boron nitride (*h*-BN) and graphene have attracted wide attention in nanoelectronics and spintronics. Since their electronic characteristics are strongly affected by the local atomic structure, the heteroatom doping could allow us to tailor the electronic and physical properties of two-dimensional materials. In this study, a non-chemical method of heteroatom doping into *h*-BN under high-energy ion irradiation was demonstrated for the LiF/*h*-BN/Cu heterostructure. Spectroscopic analysis of chemical states on the relevant atoms revealed that  $6\% \pm 2\%$  fluorinated *h*-BN is obtained by the irradiation of 2.4 MeV Cu<sup>2+</sup> ions with the fluence up to  $10^{14}$  ions cm<sup>-2</sup>. It was shown that the high-energy ion irradiation leads to a single-sided fluorination of *h*-BN by the formation of the fluorinated *sp*<sup>3</sup>-hybridized BN.

Supplementary material for this article is available [online](#)

Keywords: hexagonal boron nitride, heteroatom doping, high-energy ion irradiation, near edge x-ray absorption fine structure, *ab initio* calculation

(Some figures may appear in colour only in the online journal)

## 1. Introduction

Hexagonal boron nitride (*h*-BN) and graphene which belong to the so-called graphene's group in two-dimensional (2D) materials are expected to be applied for nanoelectronics and spintronics devices due to the novel properties like chemical and mechanical stability, quantum electronic transport,

extremely high mobility of the charge carriers and the superior insulating property [1–8]. These advantages are connected to one of the abilities of *h*-BN and graphene in which single-atom layer films with large area and high crystallinity can be synthesized by chemical vapor deposition [8–11]. In recent years, the atomic modification beyond the chemical process attracts increasing interests, which can lead to the controlled functionalization of 2D materials through the fabrications of heterostructures, heterojunctions and even

<sup>9</sup> Authors to whom any correspondence should be addressed.

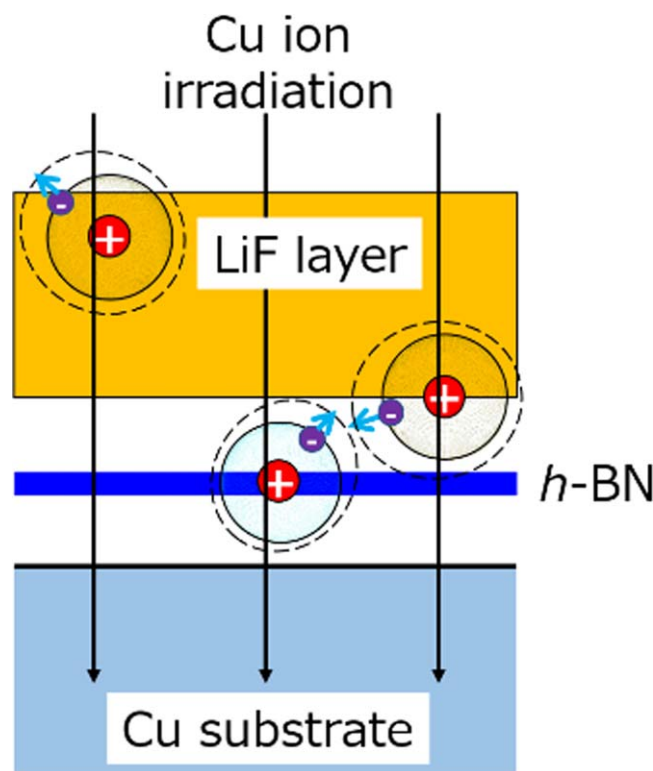
circuits in a single atomic layer sheet [12, 13], where pristine and modified regions of 2D materials are adjusted together. It is expected that heteroatom doping into *h*-BN provides superior functionalization that can be used not only for fundamental study but also for technological applications, e.g. controlling the electronic and optical properties by energy bandgap engineering, the application for the biocompatible adsorbent which works under extreme conditions by additionally introducing the water solubility, and so on [14–19]. Atomically modified graphene derivatives, such as hydrogenated graphene (graphane) [20] and fluorinated graphene (fluorographene) [21–25], have been successfully fabricated so far. In contrast, there have been scarce reports on the heteroatom doping into *h*-BN. It is only recently that a few papers about fluorinated *h*-BN have been published with the description of successful fluorination of multi-layered *h*-BN sheets by chemical routes [15, 17, 26]. Species of thermochemically dopable heteroatoms are limited in the case of *h*-BN, and in addition the heteroatom doping into the single-atomic layer with large area over a wide concentration range has not been realized in the reported method. The lower crystallinity and uniformity of the film prevent the elucidation of the atomic structure of doped *h*-BN which is necessary for functional design such as the energy bandgap and adsorption properties.

Here, we demonstrate a non-chemical route of atomistic modification of *h*-BN by employing high-energy ion irradiation. In the high-energy ion irradiation with energies exceeding several MeV, the electronic excitations are dominant compared with the energy transfer by nuclear collisions. It has been reported that the electronic excitations and/or ionizations are influential on breaking of the C–C bonds in graphene [27] and on transformation of the B–N bonds from  $sp^2$  to  $sp^3$  [28]. It is expected that, by applying high-energy ion irradiation of the bilayer structure composed of 2D material and a cover layer consisting of heteroatoms, new chemical bonds can be formed between the 2D material and the heteroatoms during the relaxation process after the electronic excitation at the interface region of the heterostructure. Given this background, we analyzed the fluorination process of monolayer *h*-BN by high-energy ion irradiation of the *h*-BN-based heterostructure in the present study. Near edge x-ray absorption fine structure (NEXAFS) spectroscopy supported by *ab initio* calculations successfully revealed that highly fluorinated *h*-BN can be synthesized superior to the defect formation by high-energy ion irradiation of the LiF/*h*-BN heterostructure. The distinct advantage of this technique is to open a general way to the functionalization of various 2D materials.

## 2. Method

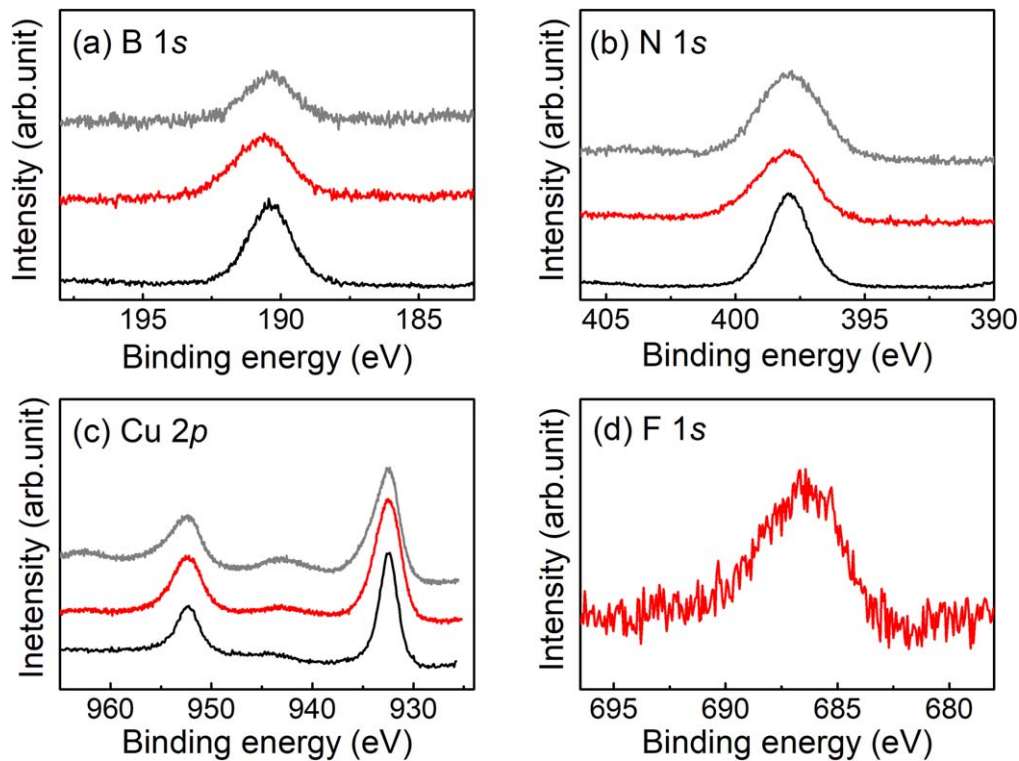
### 2.1. Materials and experimental procedure

Figure 1 shows a schematic representation of the expected atomic reaction process through ion irradiation in this study. *h*-BN specimens were synthesized on polycrystalline Cu foils



**Figure 1.** Schematic representation of atomic reaction process through ion irradiation. Red and purple spheres correspond to atomic nucleus and electrons, respectively.

by low-pressure chemical vapor deposition in a custom-designed quartz tube furnace with a base pressure of  $2 \times 10^{-6}$  Pa. The growth procedure of *h*-BN is as follows. Cu foils were introduced into the tube furnace and heated up to 1000 °C in high vacuum ( $2 \times 10^{-5}$  Pa). Hydrogen and argon gases were introduced into the furnace with pressures of 20 Pa and 50 Pa for 120 min, respectively, to remove the surface oxides from the Cu foil. Subsequently, *h*-BN was grown by exposing the Cu surface to the gas-phase reaction products of ammonia borane, including borazine vapor and hydrogen, with a pressure of 5 Pa in addition to the hydrogen and argon gases. The reaction products were obtained by heating ammonia borane at about 150 °C in a vacuum vessel connected to the tube furnace with a needle valve [29]. The generation of borazine was confirmed by quadrupole mass spectrometer (MKS, VAC-CHECK). After the *h*-BN growth, parts of the specimens were introduced to an ultrahigh vacuum chamber and a 100 nm thick LiF film was deposited on the surface of each *h*-BN/Cu specimen kept at room temperature with a Knudsen cell. The deposition rate of LiF was  $0.5 \text{ nm min}^{-1}$ . LiF was adopted as the source of F atoms due to its water-solubility, which allows removal of the LiF layer by water-rinsing after the ion irradiation. The LiF/*h*-BN/Cu specimens prepared were irradiated with 2.4 MeV  $^{63}\text{Cu}^{2+}$  ions at room temperature using a tandem-type accelerator at the Research Institute for Applied Mechanics (RIAM) in Kyushu University. The loss of the kinetic energy of the Cu ions by passing through the LiF layer is calculated to be 0.2 MeV using the SRIM code [30]. The Cu ion fluence



**Figure 2.** (a) B 1s, (b) N 1s, (c) Cu 2p and (d) F 1s core level XPS spectra of pristine *h*-BN (black),  $10^{14}$  ions  $\text{cm}^{-2}$  irradiated LiF/*h*-BN (red) and  $10^{14}$  ions  $\text{cm}^{-2}$  irradiated *h*-BN (grey). The LiF layer was removed by water-rinsing before XPS measurements.

was varied from  $10^{13}$  to  $10^{14}$  ions  $\text{cm}^{-2}$ . The electronic states and the atomic structure of *h*-BN in ion-irradiated LiF/*h*-BN/Cu specimens were analyzed by x-ray photoelectron spectroscopy (XPS), low-electron energy loss spectroscopy (LEELS) and NEXAFS spectroscopy after removing the LiF layer by rinsing with water. The XPS measurements were carried out with a hemispherical energy analyzer (VSW CLASS 100) using an Al  $K\alpha$  (1486.6 eV) x-ray source (PSP TX400/2). The LEELS measurements were performed with a double-pass cylindrical mirror analyzer (PHI 15-255G). The B and N  $K$ -edge NEXAFS measurements were carried out at the BL-8 of the SR center in Ritsumeikan University. The partial electron-yield method was employed to obtain the NEXAFS spectra. For comparison, the similar ion-irradiation and spectroscopic experiments were also performed in the *h*-BN/Cu specimens without deposition of the LiF layer.

## 2.2. Theoretical calculation

All calculations of the atomic structure were performed using DFT within the Perdew–Burke–Ernzerhof (PBE) functional [31]. We used the projector augmented wave method [32] approximation with the periodic boundary conditions implemented in the Vienna *ab initio* simulation package [33–36]. A plane-wave energy cut-off was set to 400 eV and a vacuum space of  $\sim 15$  Å was used to avoid interactions between neighboring layers. To calculate the equilibrium atomic structures the Brillouin zone was sampled according to the Monkhorst–Pack scheme [37] with a  $6 \times 6 \times 1$  grid in the  $k$ -space. The structural relaxation was performed until the forces acting

on each atom became less than  $10^{-4}$  eV/Å. NEXAFS spectra were calculated with the electron spectroscopy analysis (EISA) code [38, 39] under the assumption of the final-state one-electron approximation. The differential charge density maps were obtained with VESTA code [40].

## 3. Results and discussion

Figure 2 shows the B 1s, N 1s, Cu 2p, and F 1s core level XPS spectra of pristine *h*-BN/Cu (black), ion-irradiated LiF/*h*-BN/Cu (red) and *h*-BN/Cu (grey) with the fluence of  $10^{14}$  ions  $\text{cm}^{-2}$ . It is found that the full-width at the half maximum (FWHM) of the B 1s and N 1s peaks is broadened after the ion irradiation: the FWHM of the B 1s peak is 1.9 eV in pristine *h*-BN/Cu, 2.5 eV in ion-irradiated LiF/*h*-BN/Cu and 2.1 eV in ion-irradiated *h*-BN/Cu. The FWHM of the N 1s peak is 1.9 eV in pristine *h*-BN/Cu, 2.7 eV in ion-irradiated LiF/*h*-BN/Cu and 2.8 eV in ion-irradiated *h*-BN/Cu. It is also found that the peak position of B 1s in ion-irradiated LiF/*h*-BN/Cu is 0.3 eV higher compared with those of pristine *h*-BN/Cu and ion-irradiated *h*-BN/Cu. These changes indicate a modification of the chemical states of *h*-BN by the ion irradiation. The ion irradiation of *h*-BN/Cu leads to another impact on *h*-BN. The B 1s peak intensity of the ion-irradiated *h*-BN/Cu is approximately 0.8 times smaller than that of pristine *h*-BN/Cu, indicating a preferential desorption of B atoms by the bond breaking induced by the ion irradiation. In contrast, the B 1s peak intensity of the

ion-irradiated LiF/*h*-BN/Cu shows no significant change compared with that of pristine *h*-BN/Cu, but the peak is broadened as described above. Differences also arise in the Cu 2*p* core level spectra after the ion irradiation. In the Cu 2*p* spectra of ion-irradiated LiF/*h*-BN/Cu and *h*-BN/Cu, additional peaks appear around 943 eV. Also, the FWHM of the Cu 2*p*<sub>3/2</sub> peak is broadened from 2.0 eV in pristine *h*-BN/Cu to 2.6 eV and 3.4 eV in ion-irradiated LiF/*h*-BN/Cu and *h*-BN/Cu, respectively. The broadening of the Cu 2*p*<sub>3/2</sub> peak can be attributed to the superposition of the peaks due to metallic Cu and Cu oxidized, such as Cu<sub>2</sub>O and CuO, with slightly different binding energies [41]. The small peak at 943 eV is also attributed to Cu oxides [41]. Since these changes are remarkable in ion-irradiated *h*-BN/Cu as compared with ion-irradiated LiF/*h*-BN/Cu, it can be considered that in the *h*-BN/Cu specimens without the LiF layer the Cu foil underlying *h*-BN is easily oxidized after the ion irradiation due to the introduction of a considerable amount of vacancies in *h*-BN by the desorption of B atoms under the irradiation. In LiF/*h*-BN/Cu, the impact of the ion irradiation is different from that in *h*-BN/Cu. Figure 2(d) shows the F 1*s* core level spectrum of ion-irradiated LiF/*h*-BN/Cu after the removal of the LiF layer by water rinsing. The F 1*s* emission is seen in the spectrum and the peak is located at 686.7 eV, which is different from that of LiF (684.9 eV) [42]. It is also found that the B 1*s* and N 1*s* peaks in figures 2(a) and (b) become asymmetric towards higher binding energies. The similar additional feature has been observed in the C 1*s* spectrum of fluorinated graphene [25]. These results suggest the fluorination of *h*-BN in LiF/*h*-BN/Cu by the high-energy ion irradiation. It is calculated that the 10<sup>14</sup> ions cm<sup>-2</sup> irradiation of LiF/*h*-BN/Cu causes 6 ± 2% fluorination from the analysis of the peak intensity ratio between N 1*s* and F 1*s*. The F 1*s* peak position in ion-irradiated LiF/*h*-BN/Cu (686.7 eV) is rather comparable with that in fluorinated BN (687.5 eV) fabricated by the chemical route [26]. This also supports the fluorination of *h*-BN in ion-irradiated LiF/*h*-BN/Cu. In contrast to ion-irradiated *h*-BN/Cu without the LiF layer, the introduction of vacancies is restricted in ion-irradiated LiF/*h*-BN/Cu, since no decrease in the peak intensity of the B 1*s* spectrum and no change in the shape of the Cu 2*p* spectra are observed in the figures.

After the determination of the presence of fluorinated *h*-BN in LiF/*h*-BN/Cu, we proceed to discuss its atomic structure. Figure 3 shows the B ((a) and (b)) and N ((c) and (d)) *K*-edge NEXAFS spectra of ion-irradiated *h*-BN/Cu and LiF/*h*-BN/Cu. The incidence angles of x-ray beams to the surface are set to 30° ((a) and (c)) and 90° ((b) and (d)), respectively. The peak α is assigned to the excitations of B 1*s* and N 1*s* → π\*, respectively. The peak β and γ are assigned to the excitations of B 1*s* and N 1*s* → σ\*, respectively. It is found that the intensity of the peak α is larger at the grazing incidence (30°), while the intensities of the peaks β and γ are larger at the normal incidence (90°). This indicates that *h*-BN is oriented along the surface plane. In ion-irradiated *h*-BN/Cu (orange), a small peak at around 192.2 eV (peak i) and an intense peak at 398.2 eV (peak ii) arise in the B and N *K*-edge spectra, respectively. Although the appearance of the intense

peak such as peak ii in the N *K*-edge spectrum has not been experimentally reported for *h*-BN and its derivatives, the above spectral features are similar to those of the calculated NEXAFS based on *ab initio* modeling of *h*-BN which contains point defects with H passivation of O at the B site [43]. Since the structure of their theoretical model is different from that of our specimens (monolayer *h*-BN/Cu), we have carried out *ab initio* calculations of NEXAFS spectra based on the modified *h*-BN/Cu by replacing B atom with O atom (figure S1 is available online at [stacks.iop.org/NANO/31/125705/mmedia](https://stacks.iop.org/NANO/31/125705/mmedia)). The calculated NEXAFS spectra in figure S1 reproduce well the following spectral characteristics; the energy positions of the peaks α, β and γ, the intensity decrease of the peaks β and γ and the presence of peak i as shown in figure 3(a). In contrast, the intense peak ii in the N *K*-edge spectrum of ion-irradiated *h*-BN/Cu is not reproduced in the calculation. This is presumably due to the much lower concentration of the substituted O atom at the B site in *h*-BN in the theoretical model than in the experimental sample, which is deduced from the correlation between the ion fluence and the intensity of peak ii (see figure S2). The decrease of the amount of B atoms with the increasing of the ion fluence obtained by the XPS measurements (figure 2(a)) supports the above consideration, whereas the incorporation of O atoms is unable to be detected by XPS due to the superimposition of the several intense emissions from the oxidized Cu substrate in the O 1*s* spectrum (not shown). It is also found that the incident angle dependence of the intensity of peak ii in the N *K*-edge spectrum is much weaker compared with that of the peaks α, β and γ. This may be attributed to the deviation of the O atom positions from the basal plane of *h*-BN. From these results, it can be said that the ion irradiation of *h*-BN/Cu without the LiF layer causes the efficient introduction of defects at the B site in *h*-BN.

NEXAFS spectra of ion-irradiated LiF/*h*-BN/Cu in figure 3 show the different features from those of ion-irradiated *h*-BN/Cu. In the B *K*-edge spectrum, a peak (iii; 192.2 eV) appears at higher photon energies than the peak α (figure 3(a) inset). In the N *K*-edge spectrum, an intense peak (iv; 398.5 eV) appears at lower photon energies than the peak α, which resembles to the NEXAFS spectrum of ion-irradiated *h*-BN/Cu. However, the peak position and the peak intensity are lower compared to the spectrum of ion-irradiated *h*-BN/Cu (figure 3(c) inset). In addition to these features, the peaks β and γ are broadened in the spectra of ion-irradiated LiF/*h*-BN/Cu with the fluence higher than 5 × 10<sup>13</sup> ions cm<sup>-2</sup>. The features of the NEXAFS spectrum in ion-irradiated LiF/*h*-BN/Cu are inconsistent with those of the experimentally and theoretically obtained NEXAFS spectra in *h*-BN with various types of defects, such as C and introduced vacancies [43–45]. It can be considered that peaks iii and iv in the B and N *K*-edge spectra are caused by the transition from *sp*<sup>2</sup> to *sp*<sup>3</sup> bonding in *h*-BN based on the analogy from the similar spectral features in *h*-BN containing a mixture of *sp*<sup>2</sup> and *sp*<sup>3</sup> bonding [45]. One may suppose that the ion-irradiation of LiF/*h*-BN/Cu causes the similar changes in the atomic structure of *h*-BN as ion-irradiated *h*-BN/Cu. However, the atomic structure of *h*-BN in ion-irradiated LiF/*h*-BN/Cu is considered to be different from

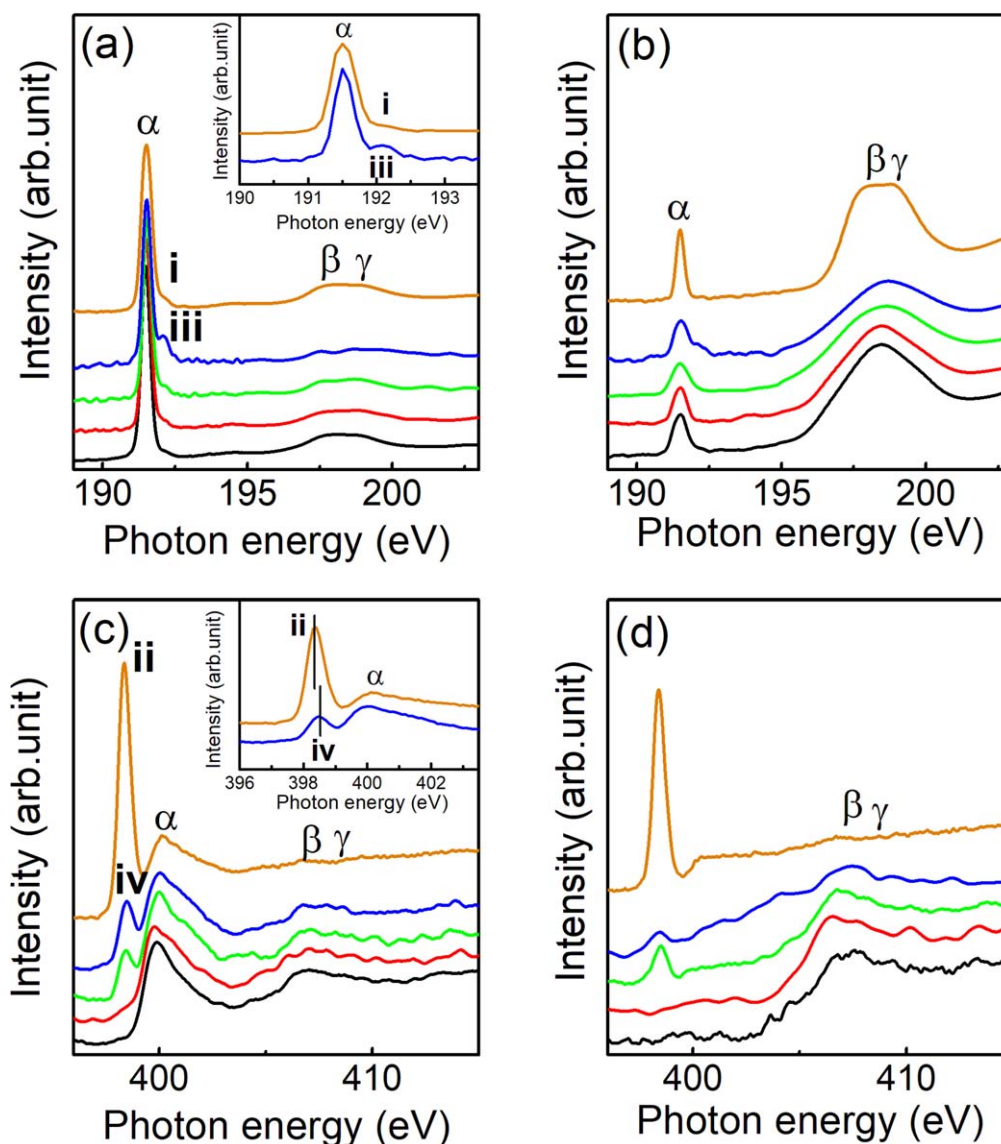


**Figure 3.** (a), (b) B *K*-edge and (c), (d) N *K*-edge NEXAFS spectra of pristine *h*-BN (black),  $10^{13}$  (red),  $5 \times 10^{13}$  (green) and  $10^{14}$  ions  $\text{cm}^{-2}$  irradiated LiF/*h*-BN (blue). For comparison, spectra of  $10^{14}$  ions  $\text{cm}^{-2}$  irradiated *h*-BN (orange) are shown in the same figures. The incident angle of x-ray beams to the surface is set to  $30^\circ$  (a), (c) and  $90^\circ$  (b), (d). The insets in (a) and (c) show the energy region at the absorption edge of the B and N *K*-edge spectra.

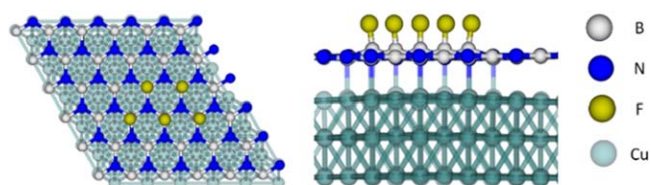


**Figure 4.** Top and side views of the proposed atomic structure of partially fluorinated *h*-BN monolayer on Cu(111) substrate. F atoms are bonded to B atoms on the irradiation side of *h*-BN. Boron, nitrogen, fluorine and copper atoms are marked by white, blue, yellow and dark green, respectively.

that in ion-irradiated *h*-BN/Cu because differences are seen between the intensity ratios of peak **i** to peak **ii** and peak **iii** to peak **iv**, and between the energy positions of peak **ii** and peak **iv**. In the similar way, the intensity ratio between the B *1s* and

N *1s* peaks is also different for ion-irradiated LiF/*h*-BN/Cu and ion-irradiated *h*-BN/Cu (figure 2). With further consideration of the adsorption of F atoms observed by XPS (figure 2(d)), it can be considered that the  $sp^3$  bonding state is originated from the formation of chemical bonding of F atoms to *h*-BN (formation of fluorinated BN). It is also found that the strong incident angle dependence of the intensity of the peak  $\alpha$  is seen even after the  $10^{14}$  ions  $\text{cm}^{-2}$  ion irradiation, which indicates a scarce change in the orientation of *h*-BN on a Cu substrate by the ion irradiation.

In order to represent the experimental samples computationally, the atomic structures of pristine *h*-BN and fluorinated *h*-BN on the Cu substrate were designed with a similar fluorine concentration (7%), as can be seen in figure 4. We suppose that the ion irradiation finally leads to the adsorption of F atoms to the *h*-BN surface with the formation of the fluorinated

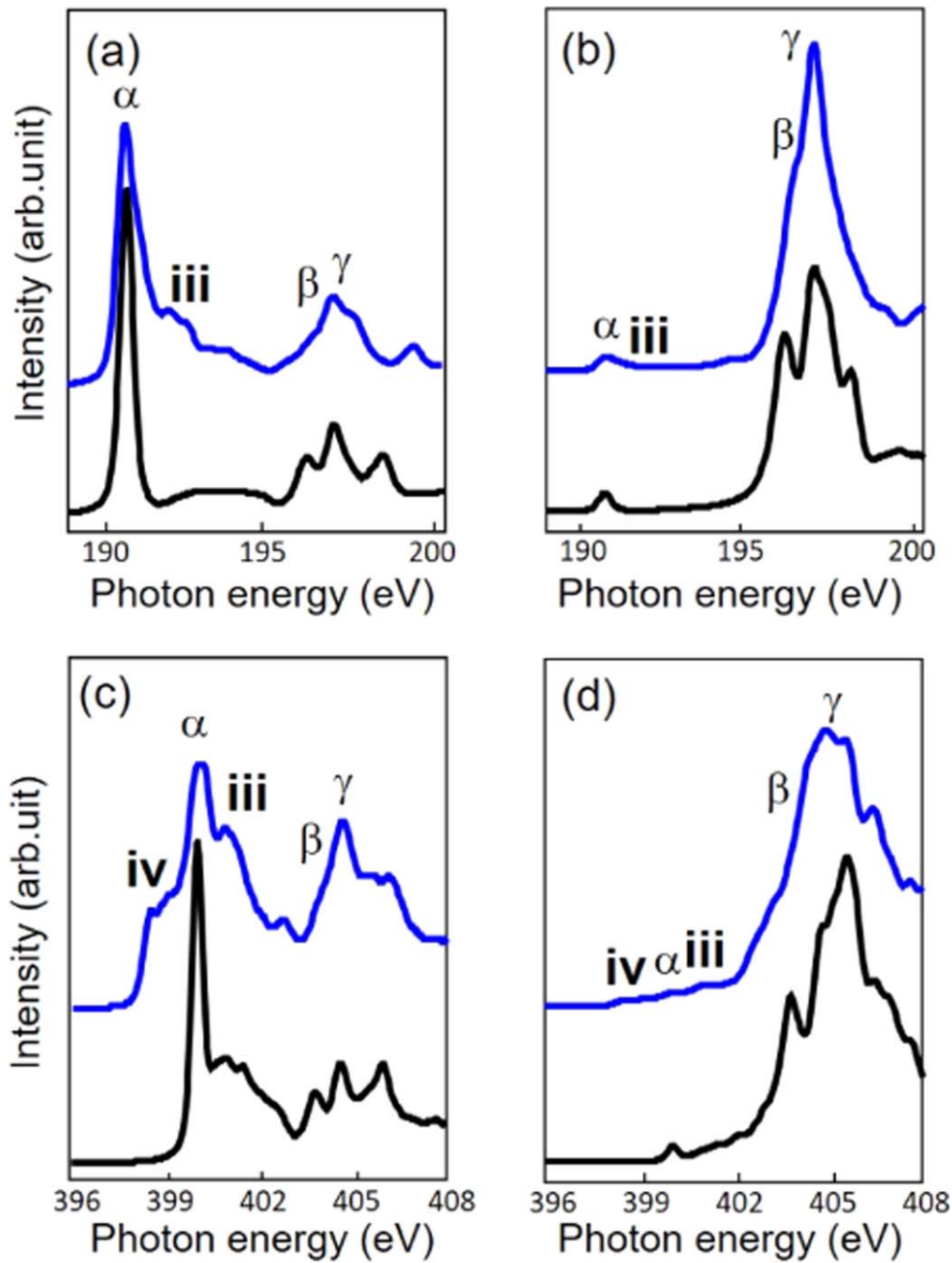


**Figure 5.** Simulated (a), (b) B *K*-edge and (c), (d) N *K*-edge NEXAFS spectra of pristine *h*-BN (black) and partially fluorinated *h*-BN (blue) on Cu substrate. The labeling of the peaks and features in simulated NEXAFS spectra ( $\alpha$ - $\gamma$ , *iii* and *iv*) corresponds to that in experimentally obtained NEXAFS spectra shown in figure 3. The angle between the polarization vector of the x-ray electric field and the normal to the sample surface was set to 30° (a), (c) and 90° (b), (d) according to experimental data.

$sp^3$ -hybridized BN. Such hybridized system could appear in *h*-BN by the nucleation mechanism as was predicted before for fluorinated graphene [46]. Being similar to the transformation of the hybridized host C atom from  $sp^2$  to  $sp^3$  in the adsorption of an F atom to graphene, a model with partially transformed *h*-BN from the  $sp^2$  to  $sp^3$  state is proposed. The essential difference between the usually considered fluorinated *h*-BN model and the structure considered in this work is the presence of the Cu substrate. It is found that the Cu substrate plays an important role in the stabilization of the one side fluorinated

structure. Indeed, the adsorption of an F atom transforms the hybridization state of the host atoms from  $sp^2$  to  $sp^3$ , which leads to the elongation of the bonds between the  $sp^3$  and  $sp^2$  hybridized atoms in the basal plane of *h*-BN and buckling of the fluorinated region. The induced local strain in the one side fluorinated BN is compensated by its bonding with the Cu substrate on the opposite side.

In order to confirm the validity of the proposed model, we compare the experimentally measured (figure 3) and theoretically calculated NEXAFS spectra of fluorinated

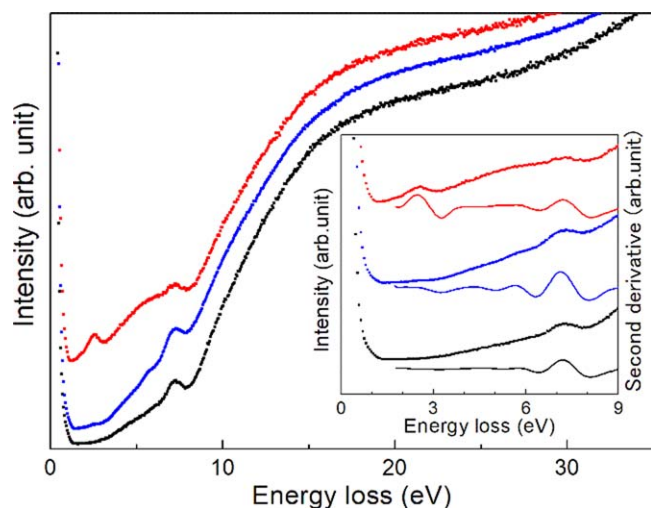


**Figure 6.** LEELS spectra of pristine *h*-BN (black),  $10^{13}$  (blue) and  $10^{14}$  ions  $\text{cm}^{-2}$  irradiated LiF/*h*-BN (red). The incident electron energy is set to 60 eV. The inset shows the LEELS spectra near the bandgap region. Solid lines show the second derivatives of pristine *h*-BN (black),  $10^{13}$  (blue) and  $10^{14}$  ions  $\text{cm}^{-2}$  irradiated LiF/*h*-BN (red) LEELS spectra.

*h*-BN/Cu (figure 5). The simulated spectra are well consistent with the experimental ones: the appearance of peak **iii** and the broadening of the peaks  $\beta$  and  $\gamma$  are reproduced. The obtained data are also supported by the perfect correspondence of the theoretically derived and experimentally measured pristine *h*-BN/Cu spectra as well as the reference data [47–49]. It has been reported that the fluorinated *h*-BN obtained by the chemical route has no site preference of F atoms to the B and N sites of *h*-BN [17], although theoretical calculations point out a strong site preference of the B site due to the large difference in electronegativity between B and N [16, 18, 50]. On the other hand, it can be said that our fluorinated *h*-BN/Cu has B–F bonds on the single side of *h*-BN in agreement with the theoretical prediction because the experimentally obtained NEXAFS spectrum is inconsistent with the simulated NEXAFS spectra of any fluorinated *h*-BN models other than the single side fluorinated variant. It is also worth noting that the B site has higher reactivity than the N site as revealed through the ion irradiation of *h*-BN/Cu without the LiF layer. This is consistent with the preferential formation of B–F bonds by the ion irradiation.

From the above discussion, it is evident that peaks **iii** and **iv** in the NEXAFS spectra appear due to the formation of fluorinated BN. Peak **iv** can be attributed to the hybridization of the  $p_z$  orbitals of BN with the  $d$  orbitals of Cu (see figure S3(a)) judging from the presence of the corresponding peak in the simulated NEXAFS spectra of pristine *h*-BN/Cu, where *h*-BN and Cu are forced to approach to a close distance for forming chemical bonding as in the case of fluorinated *h*-BN/Cu. In hydrogenated *h*-BN/Ni(111), we also find the appearance of the similar peak in the N  $K$ -edge spectrum, which has been enhanced by hydrogenation of *h*-BN [51]. In the NEXAFS spectrum of ion-irradiated *h*-BN/Cu without the LiF layer, we see the appearance of the intense peak **ii** which is 0.2 eV of photon energy lower than peak **iv**

(figure 3(c)). As discussed above, the intense peak **ii** can be attributed to the introduction of substitutional defects, indicating that peaks **ii** and **iv** have different attributions. In contrast to peak **iv**, peak **iii** can be reproduced only in the calculated spectra of fluorinated *h*-BN on the Cu substrate. One can suggest that peak **iii** occurs as a consequence of the electron density redistribution in *h*-BN due to the greater electronegativity of fluorine that attracts the electron cloud from *h*-BN. Therefore, the good correspondence between the simulated and experimentally obtained NEXAFS spectra suggests that the atomic structure of ion-irradiated LiF/*h*-BN/Cu is characterized by the presence of the locally fluorinated region bonded with the Cu atoms on the substrate under a *c*-BN like coordination.

Figure 6 shows LEELS spectra of pristine *h*-BN/Cu (black),  $10^{13}$  (blue) and  $10^{14}$  ions  $\text{cm}^{-2}$  ion-irradiated LiF/*h*-BN/Cu. The incident electron energy was set to 60 eV, which guarantees the shallow probing depth less than 0.5 nm. The obtained LEELS spectra reflect mainly the electronic structure of *h*-BN on the sample surface, although the slight contribution of the Cu substrate cannot be ignored. An intense peak at 7.3 eV and a broad structure at around 15.8 eV are assigned to the  $\pi$  and  $\pi + \sigma$  plasmon excitations, respectively [47, 52]. In the spectrum of pristine *h*-BN/Cu (black), the weak-intensity spectral features (4–6 eV) within the bandgap may be derived from the Cu substrate. After the ion irradiation, new features arise in the spectra; the peak at 2.6 eV and the broad structure at around 5 eV. It has been theoretically demonstrated that *h*-BN with point defects possesses optical absorption states within the bandgap [53]. However, the XPS and NEXAFS measurements indicate that such formation of defects with significant amounts can be ruled out in ion-irradiated LiF/*h*-BN/Cu. Therefore, it can be considered that these new structures in LEELS are originated from the mid-gap states of fluorinated BN which are related to peaks **ii** and **iv** in the NEXAFS spectra (figure 3). In addition, no change in the tail of the elastic peak (0.5–1.5 eV) with the ion fluence in the LEELS spectra is observed. This indicates the absence of inelastically scattered electrons with small energy-loss and also the preservation of the insulating nature of *h*-BN even under the fluorination.

#### 4. Conclusion

We have studied fluorination of *h*-BN by high-energy ion irradiation of the LiF/*h*-BN/Cu heterostructure. Chemical composition and electronic structure analysed by means of XPS and NEXAFS revealed that the high-energy ion irradiation of *h*-BN without the LiF layer induces point defects at the B site. In contrast, the ion irradiation of LiF/*h*-BN leads to the adsorption of F atoms to the *h*-BN surface through the formation of the fluorinated  $sp^3$ -hybridized BN. It was also found that  $6\% \pm 2\%$  fluorinated *h*-BN is obtained superior to the defect formation with the fluence up to  $10^{14}$  ions  $\text{cm}^{-2}$ . In addition, the LEELS measurements indicate the introduction of the fluorination-induced midgap states. Both experimental and theoretical analyses made clear that the ion-irradiated BN



layer displays mixed  $sp^2$  (*h*-BN) and  $sp^3$  (fluorinated BN) hybridized states, which suggests the formation of new monolayered  $sp^3$ -hybridized film that has not been obtained by chemical routes. By utilizing this non-chemical method, the non-equilibrium processing, which helps dope diverse kinds of heteroatoms as well as the high directionality and low divergence of ion beams, allows patterned doping in *h*-BN and other 2D materials.

## Acknowledgments

This work was partly supported by a Grant-in-Aid from the Ministry of Education, Culture, Sports, Science and Technology of Japan (16H03875, 17K18373, 18K13985), by the Collaborative Research Program of Research Institute for Applied Mechanics in Kyushu University (No. 27FP-22), and by the Project of Creation of Research Platforms and Sharing of Advanced Research Infrastructure. The authors are grateful to supercomputer cluster provided by Materials Modelling and Development Laboratory at NUST 'MISiS' and to the Joint Supercomputer Center of the Russian Academy of Sciences. K V L, Z I P and P B S acknowledge the financial support from the Ministry of Education and Science of the Russian Federation (Increase Competitiveness Program of NUST 'MISiS' No. K2-2019-016). P B S acknowledges the Grant of President of Russian Federation for government support of young DSc. (MD-1046.2019.2). K V L, Z I P and P B S acknowledge Dr Elena Voloshina (Humboldt-Universität, Berlin) for fruitful discussions.

## ORCID iDs

Shiro Entani  <https://orcid.org/0000-0001-9062-1123>

Masaki Mizuguchi  <https://orcid.org/0000-0003-1090-0179>

Pavel B Sorokin  <https://orcid.org/0000-0001-5248-1799>

## References

- [1] Novoselov K S, Geim A K, Morozov S V, Jiang D, Zhang Y, Dubonos S V, Grigorieva I V and Firsov A A 2004 Electric field effect in atomically thin carbon films *Science* **306** 666–9
- [2] Zhang Y, Tan Y-W, Stormer H L and Kim P 2005 Experimental observation of the quantum Hall effect and Berry's phase in graphene *Nature* **438** 201–4
- [3] Heersche H B, Jarillo-Herrero P, Oostinga J B, Vandersypen L M K and Morpurgo A F 2007 Bipolar supercurrent in graphene *Nature* **446** 56–9
- [4] Watanabe K, Taniguchi T and Kanda H 2004 Direct-bandgap properties and evidence for ultraviolet lasing of hexagonal boron nitride single crystal *Nat. Mater.* **3** 404–9
- [5] Liu Z *et al* 2013 Ultrathin high-temperature oxidation-resistant coatings of hexagonal boron nitride *Nat. Commun.* **4** 2541
- [6] Kostoglou N, Polychronopoulou K and Reibholz C 2015 Thermal and chemical stability of hexagonal boron nitride (*h*-BN) nanoplatelets *Vacuum* **112** 42–5
- [7] Li L H, Cervenka J, Watanabe K, Taniguchi T and Chen Y 2014 Strong oxidation resistance of atomically thin boron nitride nanosheets *ACS Nano* **8** 1457–62
- [8] Song L *et al* 2010 Large scale growth and characterization of atomic hexagonal boron nitride layers *Nano Lett.* **10** 3209–15
- [9] Li X *et al* 2009 Large-area synthesis of high-quality and uniform graphene films on copper foils *Science* **324** 1312–4
- [10] Entani S, Kurahashi M, Sun X and Yamauchi Y 2013 Spin polarization of single-layer graphene epitaxially grown on Ni(111) thin film *Carbon* **61** 134–9
- [11] Entani S, Takizawa M, Li S, Naramoto H and Sakai S 2019 Growth of graphene on SiO<sub>2</sub> with hexagonal boron nitride buffer layer *Appl. Surf. Sci.* **475** 6–11
- [12] Ruoff R 2008 Graphene: calling all chemists *Nat. Nanotechnol.* **3** 10–1
- [13] Chernozatonskii L A and Sorokin P B 2010 Nanoengineering structures on graphene with adsorbed hydrogen 'lines' *J. Phys. Chem. C* **114** 3225–9
- [14] Weng Q, Wang X, Wang X, Bando Y and Golberg D 2016 Functionalized hexagonal boron nitride nanomaterials: emerging properties and applications *Chem. Soc. Rev.* **45** 3989–4012
- [15] Chen S, Li P, Xu S, Pan X, Fu Q and Bao X 2018 Carbon doping of hexagonal boron nitride porous materials toward CO<sub>2</sub> capture *J. Mater. Chem. A* **6** 1832–9
- [16] Xiang H J, Yang J, Hou J G and Zhu Q 2005 Are fluorinated boron nitride nanotubes n-type semiconductors? *Appl. Phys. Lett.* **87** 243113
- [17] Radhakrishnan S *et al* 2017 Fluorinated *h*-BN as a magnetic semiconductor *Sci. Adv.* **3** e1700842
- [18] Zhang Z, Zeng X C and Guo W 2011 Fluorinating hexagonal boron nitride into diamond-like nanofilms with tunable band gap and ferromagnetism *J. Am. Chem. Soc.* **33** 14831–8
- [19] Weng Q *et al* 2017 Tuning of the optical, electronic, and magnetic properties of boron nitride nanosheets with oxygen doping and functionalization *Adv. Mater.* **29** 1700695
- [20] Elias D C *et al* 2009 Control of graphene's properties by reversible hydrogenation: evidence for graphane *Science* **323** 610–3
- [21] Nair R R *et al* 2010 Fluorographene: a two-dimensional counterpart of Teflon *Small* **6** 2877–84
- [22] Jeon K-J *et al* 2011 Fluorographene: a wide bandgap semiconductor with ultraviolet luminescence *ACS Nano* **5** 1042–6
- [23] Robinson J T *et al* 2010 Properties of fluorinated graphene films *Nano Lett.* **10** 3001–5
- [24] Şahin H, Topsakal M and Ciraci S 2011 Structures of fluorinated graphene and their signatures *Phys. Rev. B* **83** 115432
- [25] Entani S, Mizuguchi M, Watanabe H, Yu Antipina L, Sorokin P B, Avramov P V, Naramoto H and Sakai S 2016 Effective fluorination of single-layer graphene by high-energy ion irradiation through a LiF overlayer *RSC Adv.* **6** 68525–9
- [26] Xue Y, Liu Q, He G, Xu K, Jiang L, Hu X and Hu J 2013 Excellent electrical conductivity of the exfoliated and fluorinated hexagonal boron nitride nanosheets *Nanoscale Res. Lett.* **8** 49
- [27] Akcöltekin S, Bukowska H, Peters T, Osmani O, Monnet I, Alzahrer I, d'Etat B B, Lebius H and Schleberger M 2011 Unzipping and folding of graphene by swift heavy ions *Appl. Phys. Lett.* **98** 103103
- [28] Ullmann J, Baglin J E E and Kellock A J 1998 Effects of MeV ion irradiation of thin cubic boron nitride films *J. Appl. Phys.* **83** 2980–7
- [29] Frueh S, Kellett R, Mallery C, Molter T, Willis W S, King'ondo C and Suib S L 2011 Pyrolytic decomposition of ammonia borane to boron nitride *Inorg. Chem.* **50** 783–92

- [30] Ziegler J F, Ziegler M D and Biersack J P 2010 SRIM—the stopping and range of ions in matter *Nucl. Instrum. Meth. Phys. Res. B* **268** 1818–23
- [31] Perdew J P, Burke K and Ernzerhof M 1996 Generalized gradient approximation made simple *Phys. Rev. Lett.* **77** 3865–8
- [32] Blöchl P E 1994 Projector augmented-wave method *Phys. Rev. B* **50** 17953
- [33] Kresse G and Furthmüller J 1996 Efficiency of *ab initio* total energy calculations for metals and semiconductors using a plane-wave basis set *Comput. Mater. Sci.* **6** 15–50
- [34] Kresse G and Furthmüller J 1996 Efficient iterative schemes for *ab initio* total-energy calculations using a plane-wave basis set *Phys. Rev. B* **54** 11169
- [35] Kresse G and Hafner J 1993 *Ab initio* molecular dynamics for liquid metals *Phys. Rev. B* **47** 558–61
- [36] Kresse G and Hafner J 1994 *Ab initio* molecular-dynamics simulation of the liquid-metal–amorphous-semiconductor transition in germanium *Phys. Rev. B* **49** 14251
- [37] Monkhorst H J and Pack J D 1976 Special points for Brillouin-zone integrations *Phys. Rev. B* **13** 5188–92
- [38] Rajasekaran S, Abild-Pedersen F, Ogasawara H, Nilsson A and Kaya S 2013 Interlayer carbon bond formation induced by hydrogen adsorption in few-layer supported graphene *Phys. Rev. Lett.* **111** 085503
- [39] Ovcharenko R E, Tupitsyn I I, Savinov E P, Voloshina E N, Paulus B, Dedkov Y S and Shulakov A S 2013 Specific many-electron effects in x-ray spectra of simple metals and graphene *Phys. Chem. Chem. Phys.* **15** 6749–56
- [40] Momma K and Izumi F 2011 *VESTA 3* for three-dimensional visualization of crystal, volumetric and morphology data *J. Appl. Crystallogr.* **44** 1272–6
- [41] Ghijsen J, Tjeng L H, van Elp J, Eskes H, Westerink J, Sawatzky G A and Czyzyk M T 1988 Electronic structure of Cu<sub>2</sub>O and CuO *Phys. Rev. B* **38** 11322–30
- [42] Wagner C D, Riggs W M, Davis L E, Moulder J F and Muilenberg G E 1979 *Handbook of X-Ray Photoelectron Spectroscopy: A Reference Book of Standard Data for Use in X-Ray Photoelectron Spectroscopy* (Eden Prairie, MN: Perkin-Elmer Co.)
- [43] McDougall N L, Partridge J G, Nicholls R J, Russo S P and McCulloch D G 2017 Influence of point defects on the near edge structure of hexagonal boron nitride *Phys. Rev. B* **96**
- [44] Peter R, Bozanic A, Petravic M, Chen Y, Fan L-J and Yang Y-W 2009 Formation of defects in boron nitride by low energy ion bombardment *J. Appl. Phys.* **106** 083523
- [45] Jiménez I, Jankowski A F, Terminello L J, Sutherland D G J, Carlisle J A, Doll G L, Tong W M, Shuh D K and Himpsel F J 1997 Core-level photoabsorption study of defects and metastable bonding configurations in boron nitride *Phys. Rev. B* **55** 12025
- [46] Ribas M A, Singh A K, Sorokin P B and Yakobson B I 2011 Patterning nanoroads and quantum dots on fluorinated graphene *Nano Res.* **4** 143–52
- [47] Jaouen M, Hug G, Gonnet V, Demazeau G and Tourillon G 1995 An EELS and XAS study of cubic boron nitride synthesized under high pressure—high temperature conditions *Microsc. Microanal. Microstruct.* **6** 127–39
- [48] Hemraj-Benny T, Banerjee S, Sambasivan S, Fischer D A, Han W, Misewich J A and Wong S S 2005 Investigating the structure of boron nitride nanotubes by near-edge x-ray absorption fine structure (NEXAFS) spectroscopy *Phys. Chem. Chem. Phys.* **7** 1103–6
- [49] Shimoyama I, Baba Y, Sekiguchi T and Nath K G 2009 A theoretical interpretation of near edge x-ray absorption fine structure of hexagonal boron nitride monolayer on Ni(111) *J. Electron. Spectrosc. Relat. Phenom.* **175** 6–13
- [50] Zhou Z, Zhao J, Chen Z, Schleyer P and von R 2006 Atomic and electronic structures of fluorinated BN nanotubes: computational study *J. Phys. Chem. B* **110** 25678–85
- [51] Ohtomo M, Yamauchi Y, Sun X, Kuzubov A A, Mikhaleva N S, Avramov P V, Entani S, Matsumoto Y, Naramoto H and Sakai S 2017 Direct observation of site-selective hydrogenation and spin-polarization in hydrogenated hexagonal boron nitride on Ni(111) *Nanoscale* **9** 2369–75
- [52] Arenal R, Stéphan O, Kociak M, Taverna D, Loiseau A and Colliex C 2005 Electron energy loss spectroscopy measurement of the optical gaps on individual boron nitride single-walled and multiwalled nanotubes *Phys. Rev. Lett.* **95** 127601
- [53] Ngwenya T B, Ukpong A M and Chetty N 2011 Defect states of complexes involving a vacancy on the boron site in boronitrene *Phys. Rev. B* **84** 245425